Full-film dry transfer of MBE-grown van der Waals materials

To cite this article: Ziling Li *et al* 2025 *2D Mater.* **12** 035003

IOP Publishing 2D Mater. 12 (2025) 035003 https://doi.org/10.1088/2053-1583/adc611

2D Materials

PAPER

Full-film dry transfer of MBE-grown van der Waals materials

Ziling Li, Wenyi Zhou, Matthew Swann, Vika Vorona, Haley Scott and Roland K Kawakami*

Department of Physics, The Ohio State University, Columbus, OH 43210, United States of America
* Author to whom any correspondence should be addressed.

E-mail: kawakami.15@osu.edu

Keywords: large-area transfer, molecular beam epitaxy, dry transfer, 2D magnets, topological insulators, transition metal dichalcogenides

Supplementary material for this article is available online

OPEN ACCESS

RECEIVED
12 February 2025

REVISED
18 March 2025

ACCEPTED FOR PUBLICATION
27 March 2025

PUBLISHED
7 April 2025

Abstract

Molecular beam epitaxy (MBE) has been used to create high-quality, large-scale two-dimensional van der Waals (2D vdW) materials. However, due to the strong adhesion between the substrate and deposited materials, the peel-off and dry transfer of MBE-grown vdW films onto other substrates has been challenging. This limits the study and use of MBE films for heterogeneous integration including stacked and twisted heterostructures. In this work, we develop a polymer-assisted dry transfer method and successfully perform full-film transfer of various MBE-grown 2D vdW materials including transition metal dichalcogenides, topological insulators and 2D magnets. In particular, we transfer air-sensitive 2D magnets, characterize their magnetic properties, and compare them with as-grown materials. The results show that the transfer technique does not degrade the magnetic properties, with the Curie temperature and hysteresis loops exhibiting similar behaviors after the transfer. Our results enable further development of heterogeneous integration of 2D vdW materials based on MBE growth.

1. Introduction

Two-dimensional van der Waals (2D vdW) materials and their heterostructures have received significant attention due to their unique electronic, optical, and magnetic properties, which make them promising candidates for applications in fields such as nanoelectronics [1], optoelectronics [2] and spintronics [3]. Traditional methods for creating these heterostructures, such as mechanical exfoliation and top–down stacking [4, 5], have limitations in scalability and reproducibility. To address these challenges, researchers have turned to bottom-up growth techniques such as chemical vapor deposition (CVD) [6] and molecular beam epitaxy (MBE) [7] to produce large-scale 2D materials.

Both CVD and MBE have demonstrated the ability to grow high-quality materials. MBE specifically offers a number of advantages including precise doping control [8], the ability to grow complex structures [9], non-equilibrium growth of metastable phases [10–12], epitaxial alignment with the substrate, *in situ* growth monitoring by electron diffraction, and excellent crystal quality [13]. However, a critical limitation of MBE lies in its difficulty with fabrication of stacked and twisted heterostructures, which have been achieved with exfoliated [14–16] and CVD-grown materials [17] through polymer-assisted dry transfer. MBE-grown films often exhibit strong adhesion to their substrates [18], making them more difficult to peel off and dry transfer than CVD-grown films. A successful release and large-area dry transfer of MBE films while maintaining high quality would open many possibilities for stacked vdW heterostructures, hybrid structures with other materials (e.g. oxides, nitrides), and free-standing membranes.

In this work, we introduce a novel polymer-assisted dry transfer method utilizing polycaprolactone (PCL) to realize the large-area peel-off and transfer of various MBE-grown 2D vdW materials. The technique has demonstrated full-film peeling with area limited by the substrate size (up to 5×5 mm^2 so far) and has a high area yield ($> 90\%$) based on the

optical images, which is comparable to reported area yields in the studies of dry transfer of CVD films [19, 20]. We have successfully transferred 2D semiconductors ($MoSe_2$, WSe_2), topological insulators (TIs) (Bi_2Se_3, Bi_2Te_3), and 2D magnets (Fe_3GeTe_2). To test the material quality, we compare the magnetic properties of Fe_3GeTe_2 before and after the transfer and find that both the Curie temperature and the coercivity show similar behaviors. This dry transfer method not only preserves the intrinsic properties of the materials but also facilitates the development of heterogeneous integration of 2D vdW materials based on MBE growth. Our findings represent a significant advancement in the field, offering a reliable and scalable approach for fabricating high-quality 2D material heterostructures.

2. Experimental results

Over the past decade, polymer-assisted dry transfer of exfoliated and CVD-grown 2D materials has utilized PC and PPC for the transfer [4, 21–24]. More recently, PCL was introduced for dry transfer of exfoliated flakes, which benefits from stronger adhesion and lower transfer temperatures compared to PC and PPC [25, 26]. In addition, PCL can be easily dissolved by tetrahydrofuran (THF), leaving a cleaner surface compared to conventional poly(methyl methacrylate) (PMMA) [23] and similar cleanness as PC and PPC [26]. These properties make PCL an ideal candidate for transferring MBE-grown vdW layers.

Figure 1(a) illustrates the schematic of the peel-off process. We utilized a 5% solution (by weight) of PCL (Sigma Aldrich, average M_n: 80 000) in THF (Sigma Aldrich, $\geqslant$99.9% anhydrous) and spin-coated at 1000 rpm for 1 min and subsequently baked at 75 °C for 5 min to form a uniform PCL layer on top of the MBE-grown vdW film. A piece of thermal release tape (TRT, Nitto Denko Corp, Revalpha RA-95LS(N)), followed by a polydimethylsiloxane (PDMS, Gel-Pak) stamp, is gently pressed onto the PCL film to provide mechanical support. After cooling to room temperature, the entire structure is then slowly peeled off (~30–60 s for a 5 mm × 5 mm film) using a roller (3D printed using polylactic acid) with a small detachment angle to prevent cracking during the process. Due to the stronger adhesion between the PCL and the MBE-grown vdW film compared to the substrate, a uniform vdW film is successfully peeled, as demonstrated by the example of Fe_3GeTe_2/Bi_2Te_3 (FGT/BT) in figures 1(b) and (c).

To deposit the MBE film onto the target substrate, as shown in the schematic in figure 1(d), the PDMS/TRT/PCL stamp is mounted onto a micromanipulator for precise alignment with the target substrate. A two-step heating process is employed during the drop-down procedure. First, the stamp is approached to the target substrate at 50 °C while gradually increasing the substrate temperature to 65 °C. During this step, the PCL layer gradually melts and spreads across the contact region, minimizing the formation of bubbles between the vdW material and the substrate. This results in a flat and uniform surface of the transferred film. Once the vdW film is fully attached, the temperature is further increased to 90 °C to thermally release the PCL/vdW layer. Since 90 °C is in between the melting temperature of PCL (~75 °C) and TRT release temperature (~105 °C), only PCL will melt down and TRT residue is negligible. Finally, the PCL layer is removed using THF solvent, leaving behind a clean and well-transferred film, as exemplified by the FGT/BT film on a SiO_2(thickness of 285 nm)/Si substrate in figures 1(e) and (f).

For developing this process, we have systematically tested various configurations of the lifting components. When only PCL and TRT are utilized, as illustrated in figure 2(a), the peeled-off and transferred BT film exhibits patchy coverage (figure 2(b)). Introducing a PDMS layer atop the TRT/PCL stack as a supporting layer (figure 2(c)) significantly improves the peel-off and transfer processes, yielding BT films with enhanced coverage (figure 2(d)). However, residual wrinkles, cracks, and holes persist in the transferred film. Attributing this improvement to the added rigidity provided by the PDMS during peel-off, we further incorporate a rigid 3D-printed cylindrical roller (figure 2(e)) with a large radius of curvature (~20 cm). A small detachment angle θ is maintained to minimize tensile and buckling strain during peeling, ultimately achieving a uniform and crack-free transfer, as demonstrated in figure 2(f). In practice, our roller is not a full cylinder as depicted schematically in figure 1(a), but is a smaller segment of the cylindrical surface (a few cm in length) to accommodate a large radius curvature for a small detachment angle.

To explore the universality of PCL transfer, we apply the PCL transfer to different MBE-grown vdW materials including transition metal dichalcogenides (TMD) $MoSe_2$ and WSe_2, TI Bi_2Se_3 and Bi_2Te_3, and 2D magnet Fe_3GeTe_2. In figure 3, the film thicknesses are 9 layers of Bi_2Se_3 (~9 nm), 14 layers of Bi_2Te_3 (~14 nm), 3 layers of $MoSe_2$ (~2 nm), and 13 layers of WSe_2 (~9 nm). The Fe_3GeTe_2 sample consists of 8 layers of Fe_3GeTe_2 on 10 layers of Bi_2Te_3 and is capped with 5 nm of CaF_2 (total thickness of ~21 nm). Details of the MBE growths are in the Supplementary Material [27]. All the materials show good transfer results which indicates the PCL transfer method can be employed for a variety of 2D vdW materials. To further evaluate the surface quality of the transferred film, we performed atomic force microscopy (AFM) measurements on uncapped vdW films before (figures 3(a)–(e)) and after transfer

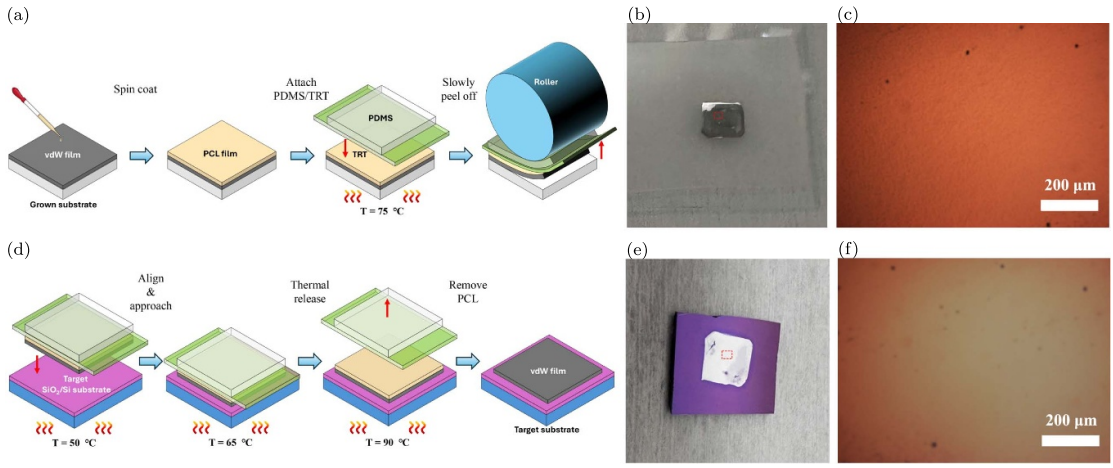

Figure 1. Process for PCL transfer of vdW films. (a) Schematic diagram of peeling off vdW film from the growth substrate. (b) Photograph of peeled FGT/BT film on the TRT/PDMS stamp (face up). (c) Microscopic optical image of the red dashed box region in (b). (d) Schematic diagram of transferring vdW film onto the target substrate. (e) Photograph of transferred FGT/BT film on the SiO_2/Si substrate. (f) Microscopic optical image of the red dashed box region in (e).

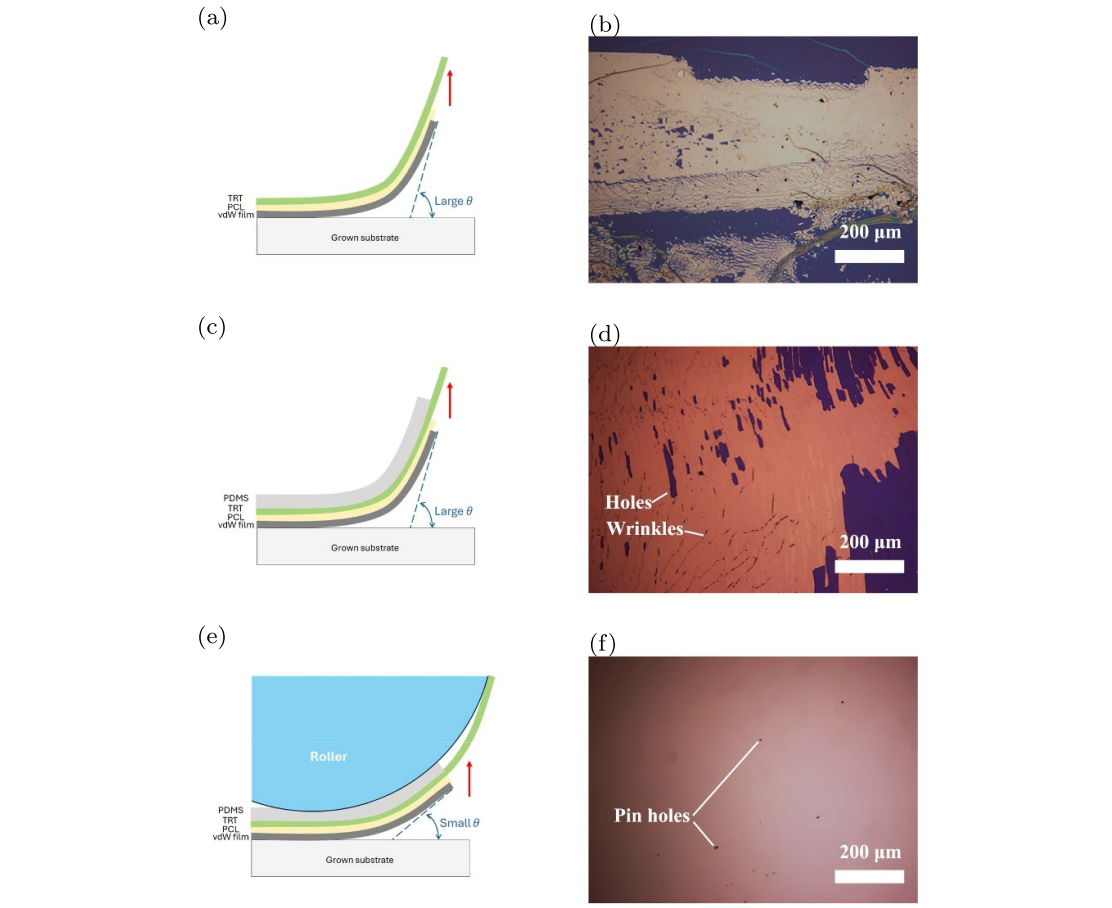

Figure 2. Peel-off and transfer development. (a) Schematic diagram using only TRT/PCL. (b) Microscopic optical image of BT film transferred onto SiO_2/Si. (c) and (d) Schematic diagram and microscope image by adding a PDMS support layer. (e) and (f) Schematic diagram and microscope image by adding a roller.

(figures 3(f)–(j)). Figure 3(k) shows that the samples have comparable root-mean-squared (RMS) roughness before and after transfer, ranging from 0.8 nm to 1.6 nm. The increase of RMS is about 1 nm, which is better than traditional PMMA-based transfer (∼5 nm) and is comparable to optimized transfer of CVD-grown materials [23, 28]. While it may appear that the roughness increases more for Fe_3GeTe_2, $MoSe_2$, and

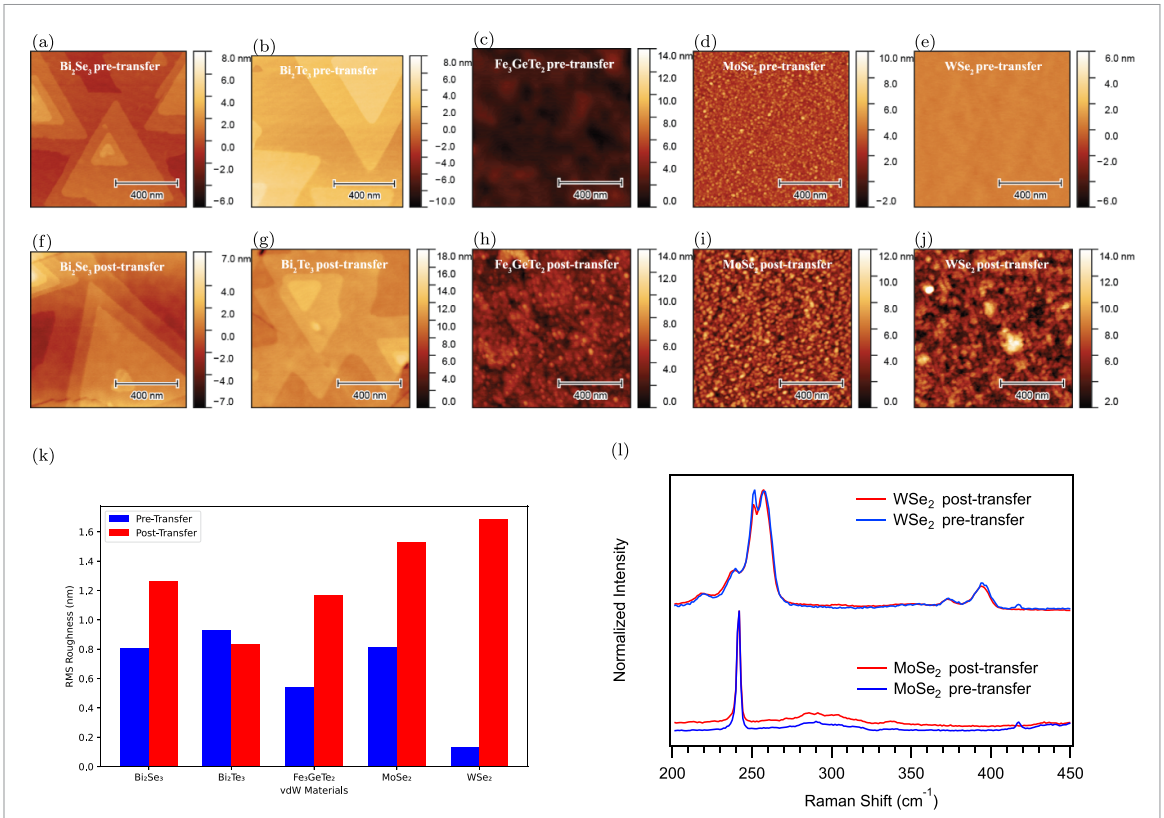

Figure 3. Gallery of transferred vdW materials. (a)–(e) AFM images of as-grown Bi_2Se_3, Bi_2Te_3, Fe_3GeTe_2, $MoSe_2$ and WSe_2 on c-sapphire substrates. (f)–(j) AFM images of transferred Bi_2Se_3, Bi_2Te_3, Fe_3GeTe_2, $MoSe_2$ and WSe_2 on SiO_2/Si substrates. (k) Statistics of RMS surface roughness of vdW films before (blue) and after (red) PCL transfer. (l) Raman spectra of $MoSe_2$ and WSe_2 before (blue) and after (red) PCL transfer. The intensities are normalized for better comparison.

WSe_2, we have not observed any obvious trends based on the material or initial roughness. In practice, an important factor is the quality of the drop-down step (figure 1(d)), which could result in trapped bubbles and wrinkles [21].

To examine the material quality of the transferred film, we also measure Raman spectra of $MoSe_2$ and WSe_2 before and after PCL transfer using a Renishaw inVia confocal Raman microscope. Raman directly probes the lattice vibrational modes for a given material and is sensitive to the crystallinity of the film. It is expected that as the crystalline quality deteriorates, the linewidth will increase and the peak positions may change [29–31]. Spectra are collected using a 633 nm excitation source transmitted through a 50 × lens located above the sample, along with a 1800 lines mm^{-1} grating and a CCD detector. Raman spectroscopy of $MoSe_2$ and WSe_2 before and after transfer yields nearly identical spectra. The widths and peak positions before and after remain largely unchanged, with only a small decrease in intensity of the e_g peak for WSe_2 at 251 cm^{-1} relative to other modes [32], confirming the films' crystalline quality remains stable through the transfer process.

Next, we demonstrate the transfer of a complex 2D magnet/TI heterostructure [9] and compare the magnetic properties before and after transfer. The FGT/BT film is capped with 10 nm of Te to prevent oxidation after MBE growth (See supplementary [27]). We transfer the Te/FGT/BT film from the c-sapphire substrate to SiO_2/Si substrate using the PCL transfer method in air. To investigate the influence of transfer on the magnetic properties, we perform reflective magnetic circular dichroism (MCD) to measure out-of-plane magnetic hysteresis loops of the Te/FGT/BT heterostructures before and after transferring. Samples are loaded into an optical cryostat (Advanced Research Systems, DMX-20-OM) to control the temperature. We utilize a continuous wave 532 nm laser with power of 100 μW focused onto a $\sim$3 μm-diameter spot using a 50× microscope objective at normal incidence. The polarization of the incident light is modulated between left-circularly polarized (LCP) and right-circularly polarized (RCP) by a photoelastic modulator (Hinds Instrument) at a frequency of 59 kHz. The reflected beam intensity (I) is measured by a photodiode detector (Thorlabs PDA36A2) and the MCD ratio $(I_{RCP} - I_{LCP})/(I_{RCP} + I_{LCP})$ is extracted by a lock-in amplifier (Signal Recovery 7270). A magnetic field is applied by a vector electromagnet to apply an out-of-plane magnetic field. The magnet is controlled by a data acquisition card (National Instruments PCIe-6323), which enables a relatively high ramp rate of

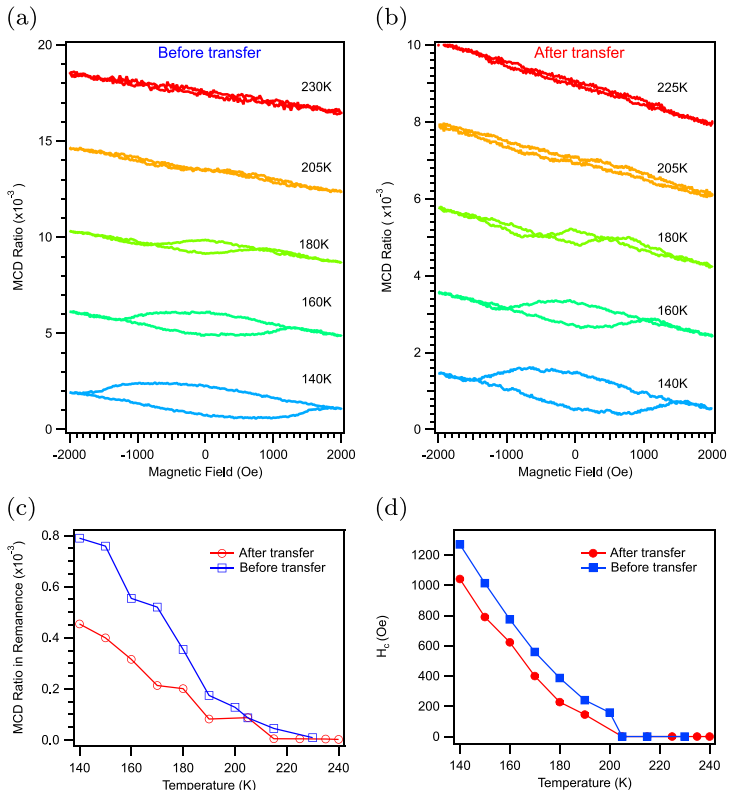

Figure 4. Magnetic properties of FGT/BT films: (a) Temperature dependence of MCD loops for FGT/BT sample before transfer. (b) Temperature dependence of MCD loops for FGT/BT sample after transfer.(c) Temperature dependence of extracted MCD ratio in remanence. (d) Temperature dependence of extracted coercive field H_c.

400 Oe s^{-1} to avoid drift of the MCD signal. The presented MCD hysteresis loops are typically averaged over 10–20 scans, and the loops have been antisymmetrized, i.e. $MCD^{anti}_{up}(H) = \frac{1}{2}[\mathrm{MCD}_{up}(H) - \mathrm{MCD}_{down}(-H)]$, $\mathrm{MCD}^{anti}_{down}(H) = \frac{1}{2}[\mathrm{MCD}_{down}(H) - \mathrm{MCD}_{up}(-H)]$, where 'up' and 'down' refer to the field sweep direction.

Figure 4 compares the magnetic properties before and after the transfer. Prior to the transfer, out-of-plane magnetic hysteresis loops are measured by MCD at a series of temperatures (figure 4(a)). At 140 K, the hysteresis loop exhibits a large coercivity, H_c, of ∼1200 Oe. At lower temperatures, the sample cannot be fully saturated with the electromagnet (∼2000 Oe maximum field). Above 140 K, H_c decreases with increasing temperature, and the magnetic hysteresis loop disappears by ∼200 K. Figure 4(b) shows the corresponding data after the FGT/BT has been transferred onto a SiO_2/Si substrate. Here, the behavior is similar to the as-grown sample, with the magnetization preserving its perpendicular orientation and the magnetic hysteresis loop disappearing by ∼200 K. However, H_c is slightly reduced compared to the as-grown sample.

Figures 4(c) and (d) plot the MCD ratio in remanence and coercivity, respectively, as a detailed function of temperature and provide a comparison before and after the transfer. The most noticeable difference is the magnitude of the MCD ratio in remanence, which is likely a consequence of the optical properties as opposed to changes in the magnetic properties. For instance, the presence of the ∼285 nm thick SiO_2 layer on the Si substrate creates an optical interference effect that could modify the magneto-optic response. Nevertheless, in both cases the MCD signal disappears above ∼200 K, signifying that the Curie temperature is largely preserved. For the coercivity before and after the transfer, H_c decreases with increasing temperature and disappears at the Curie temperature. However, the magnitudes of H_c are slightly smaller after the transfer. In summary, the Curie temperature and perpendicular magnetization orientation remain unchanged after transferring, and although there are small changes to H_c due to the transfer, we are highly encouraged that the magnetic properties are largely preserved overall.

Lastly, we provide some practical comments that may be helpful but have not yet been studied systematically. First, the time between growth and transfer could have an impact on the success of transfer, and this likely depends on the material. For example, we have been unable to peel off Bi_2Se_3 and Bi_2Te_3 if the film is more than a couple of weeks old, even if it has been stored in a dry nitrogen box and regardless

of whether it was capped. On the other hand, the $MoSe_2$ shown in figure 3 was transferred successfully even though it was stored in a dry nitrogen box for ∼6 months and did not have a protective capping layer. Second, we have studied samples in the thickness range between 3 and 20 vdW layers so far, and we have achieved successful transfer in this range. We have not yet attempted thinner films, mainly because most of our stored films are thicker than a few vdW layers in order to have full coverage without holes (e.g. see [33]). However, we anticipate that the transfer should work in the monolayer regime. Third, the ∼20 cm radius of curvature for the cylindrical surface of the roller is the first value that we have tried, and it has not yet been optimized. Other curvatures may lead to higher area yields. Fourth, while this transfer approach is scalable in principle, we have only tested it for samples of size ∼5 mm × 5 mm. In going to larger sizes, we anticipate that the peeling step could remain similar, but the drop-down step might require modifications due to the increased possibility of trapping gases and forming bubbles. For example, the drop-down step might benefit from being performed under vacuum. These are a few ways to further improve this dry transfer technique for MBE-grown vdW films.

3. Conclusion

In conclusion, we have developed a polymer-assisted dry transfer method utilizing PCL to enable the robust, large-area transfer of MBE-grown van der Waals materials, overcoming the critical challenge of strong substrate adhesion inherent to epitaxial films. By optimizing the interplay between PCL adhesion, thermal release tape, and PDMS mechanical support, we have achieved a high area yield transfer of air-sensitive 2D magnets, TIs, and semiconductors onto arbitrary substrates. Atomic force microscopy and Raman spectroscopy confirm the preservation of the structural integrity, with the increase in RMS roughness from the transfer limited to ∼1 nm, surpassing conventional PMMA-based methods. Crucially, MCD measurements reveal negligible changes in the Curie temperature of FGT/BT heterostructures, underscoring the method's compatibility with delicate magnetic and electronic states. The universality of this technique, validated across diverse material systems, bridges the gap between high-quality MBE growth and functional device integration, opening opportunities for twisted heterostructures, hybrid quantum devices, and freestanding membranes. Future efforts could focus on scaling the process to wafer-sized substrates and exploring novel heterostructures for spintronic, quantum, and optoelectronic applications. Our results establish a robust platform for advancing the heterogeneous integration of 2D materials, paving the way for next-generation van der Waals technologies.

Data availability statement

The data that support the findings of this study are openly available at the following URL/DOI: https://doi.org/10.5281/zenodo.14860478.

Conflicts of interest

The authors declare no conflict of interest.

Acknowledgments

The research was primarily supported by the U.S. Department of Energy, Office of Science, Basic Energy Sciences under Award Number DE-SC0016379 (Z L and R K K). W Z acknowledges support from the Center for Energy Efficient Magnonics, an Energy Frontiers Research Center funded by the U.S. Department of Energy, Office of Science, Basic Energy Sciences under Award Number DE-AC02-76SF00515 and the AFOSR/MURI Project 2DMagic under award number FA9550-19-1-0390 (for MBE growth, MCD, XRD, and AFM of TIs and 2D magnets). M T S acknowledges support from Intel CAFÉ (for MBE growth, Raman, and AFM of TMDs). Partial funding for shared facilities used in this research was provided by the Center for Emergent Materials: an NSF MRSEC under award number DMR-2011876.

ORCID iDs

Ziling Li https://orcid.org/0000-0002-0353-7036
Wenyi Zhou https://orcid.org/0000-0001-9717-5955
Matthew Swann https://orcid.org/0009-0005-9477-5847
Vika Vorona https://orcid.org/0009-0004-6339-8340
Haley Scott https://orcid.org/0009-0009-8122-4914
Roland K Kawakami https://orcid.org/0000-0003-0245-9192

References

[1] Lemme M C, Akinwande D, Huyghebaert C and Stampfer C 2022 2D materials for future heterogeneous electronics *Nat. Commun.* **13** 1392
[2] Tan T, Jiang X, Wang C, Yao B and Zhang H 2020 2D material optoelectronics for information functional device applications: status and challenges *Adv. Sci.* **7** 2000058
[3] Ahn E C 2020 2D materials for spintronic devices *npj 2D Mater. Appl.* **4** 17
[4] Purdie D G, Pugno N, Taniguchi T, Watanabe K, Ferrari A and Lombardo A 2018 Cleaning interfaces in layered materials heterostructures *Nat. Commun.* **9** 5387
[5] Guo H-W, Hu Z, Liu Z-B and Tian J-G 2021 Stacking of 2D materials *Adv. Funct. Mater.* **31** 2007810
[6] Cai Z, Liu B, Zou X and Cheng H-M 2018 Chemical vapor deposition growth and applications of two-dimensional materials and their heterostructures *Chem. Rev.* **118** 6091

[7] Maurtua C, Zide J and Chakraborty C 2024 Molecular beam epitaxy and other large-scale methods for producing monolayer transition metal dichalcogenides *J. Phys.: Condens. Matter* **36** 383003
[8] Wang B, Xia Y, Zhang J, Komsa H-P, Xie M, Peng Y and Jin C 2020 Niobium doping induced mirror twin boundaries in MBE grown WSe_2 monolayers *Nano Res.* **13** 1889
[9] Zhou W *et al* 2023 Tuning the Curie temperature of a two-dimensional magnet/topological insulator heterostructure to above room temperature by epitaxial growth *Phys. Rev. Mater.* **7** 104004
[10] Zhang J L *et al* 2016 Epitaxial growth of single layer blue phosphorus: a new phase of two-dimensional phosphorus *Nano Lett.* **16** 4903
[11] Chen H-D and Lin D-S 2016 Ordered 2D structure formed upon the molecular beam epitaxy growth of Ge on the silicene/Ag (111) surface *ACS Omega* **1** 357
[12] Reis F, Li G, Dudy L, Bauernfeind M, Glass S, Hanke W, Thomale R, Schäfer J and Claessen R 2017 Bismuthene on a SiC substrate: a candidate for a high-temperature quantum spin Hall material *Science* **357** 287
[13] Dimoulas A 2022 Perspectives for the growth of epitaxial 2D van der Waals layers with an emphasis on ferromagnetic metals for spintronics *Adv. Mater. Int.* **9** 2201469
[14] Geim A K and Grigorieva I V 2013 Van der Waals heterostructures *Nature* **499** 419
[15] Novoselov K S, Mishchenko A, Carvalho A and Castro Neto A H 2016 2D materials and van der Waals heterostructures *Science* **353** aac9439
[16] Kennes D M, Claassen M, Xian L, Georges A, Millis A J, Hone J, Dean C R, Basov D N, Pasupathy A N and Rubio A 2021 Moiré heterostructures as a condensed-matter quantum simulator *Nat. Phys.* **17** 155
[17] Watson A J, Lu W, Guimarães M H and Stöhr M 2021 Transfer of large-scale two-dimensional semiconductors: challenges and developments *2D Mater.* **8** 032001
[18] Mavridi N, Zhu J, Eldose N M, Prior K A and Moug R T 2018 Adhesion measurements of epitaxially lifted MBE-grown ZnSe *J. Electron. Mater.* **47** 4394
[19] Thakur M, Macha M, Chernev A, Graf M, Lihter M, Deen J, Tripathi M, Kis A and Radenovic A 2020 Wafer-scale fabrication of nanopore devices for single-molecule DNA biosensing using MoS_2 *Small Methods* **4** 2000072
[20] Wang P, Song S, Najafi A, Huai C, Zhang P, Hou Y, Huang S and Zeng H 2020 High-fidelity transfer of chemical vapor deposition grown 2D transition metal dichalcogenides via substrate decoupling and polymer/small molecule composite *ACS Nano* **14** 7370
[21] Pizzocchero F, Gammelgaard L, Jessen B S, Caridad J M, Wang L, Hone J, Bøggild P and Booth T J 2016 The hot pick-up technique for batch assembly of van der Waals heterostructures *Nat. Commun.* **7** 11894
[22] Lin Y-C, Jin C, Lee J-C, Jen S-F, Suenaga K and Chiu P-W 2011 Clean transfer of graphene for isolation and suspension *ACS Nano* **5** 2362
[23] Mondal A, Biswas C, Park S, Cha W, Kang S-H, Yoon M, Choi S H, Kim K K and Lee Y H 2024 Low Ohmic contact resistance and high on/off ratio in transition metal dichalcogenides field-effect transistors via residue-free transfer *Nat. Nanotechnol.* **19** 34
[24] Zhao Y *et al* 2022 Large-area transfer of two-dimensional materials free of cracks, contamination and wrinkles via controllable conformal contact *Nat. Commun.* **13** 4409
[25] Son S *et al* 2020 Strongly adhesive dry transfer technique for van der Waals heterostructure *2D Mater.* **7** 041005
[26] Park G, Son S, Kim J, Chang Y, Zhang K, Kim M, Lee J and Park J-G 2024 New twisted van der Waals fabrication method based on strongly adhesive polymer *2D Mater.* **11** 025021
[27] Supplemental Material for details on the MBE growth, RHEED patterns, and XRD measurements. This includes [34–36]
[28] Han Y, Zhang L, Zhang X, Ruan K, Cui L, Wang Y, Liao L, Wang Z and Jie J 2014 Clean surface transfer of graphene films via an effective sandwich method for organic light-emitting diode applications *J. Mater. Chem.* **2** 201
[29] Lee T, Mas'ud F A, Kim M J and Rho H 2017 Spatially resolved Raman spectroscopy of defects, strains and strain fluctuations in domain structures of monolayer graphene *Sci. Rep.* **7** 16681
[30] Mignuzzi S, Pollard A J, Bonini N, Brennan B, Gilmore I S, Pimenta M A, Richards D and Roy D 2015 Effect of disorder on Raman scattering of single-layer MoS_2 *Phys. Rev.* B **91** 195411
[31] Neumann C *et al* 2015 Raman spectroscopy as probe of nanometre-scale strain variations in graphene *Nat. Commun.* **6** 8429
[32] del Corro E, Terrones H, Elias A, Fantini C, Feng S, Nguyen M A, Mallouk T E, Terrones M and Pimenta M A 2014 Excited excitonic states in 1L, 2L, 3L, and bulk WSe_2 observed by resonant Raman spectroscopy *Acs Nano* **8** 9629
[33] Goff B M, Zhou W, Bishop A J, Bailey-Crandell R, Robinson K, Kawakami R K and Gupta J A 2024 Scanning tunneling microscopy study of epitaxial Fe_3GeTe_2 monolayers on Bi_2Te_3 *2D Mater.* **11** 025012
[34] Levy I, Garcia T A, Shafique S and Tamargo M C 2018 Reduced twinning and surface roughness of Bi_2 Se_3 and Bi_2Te_3 layers grown by molecular beam epitaxy on sapphire substrates *J. Vacuum Sci. Technol.* B **36** 02D107
[35] Harrison S E, Li S, Huo Y, Zhou B, Chen Y L and Harris J S 2013 Two-step growth of high quality Bi_2Te_3 thin films on Al_2O_3(0001) by molecular beam epitaxy *Appl. Phys. Lett.* **102** 171906
[36] Nakano M, Wang Y, Kashiwabara Y, Matsuoka H and Iwasa Y 2017 Layer-by-layer epitaxial growth of scalable WSe_2 on sapphire by molecular beam epitaxy *Nano Lett.* **17** 5595